TECHNICAL RESEARCH REPORT

SYSTEMS RESEARCH CENTER

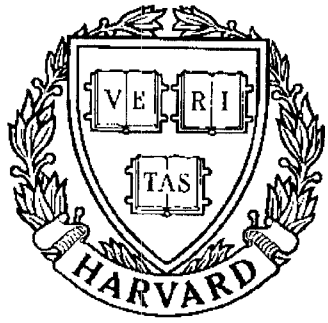

Supported by the National Science Foundation Engineering Research Center Program (NSFD CD 8803012), the University of Maryland, Harvard University, and Industry

Almost Poisson Integration of Rigid Body Systems

by M. Austin, P.S. Krishnaprasad, L.-S. Wang

TR 91-45r1

Almost Poisson Integration of Rigid Body Systems[1]

Mark Austin[2], P.S. Krishnaprasad[3], L.-S. Wang[4]

Systems Research Center,
University of Maryland,
College Park, MD 20742.

Abstract

In this paper we discuss the numerical integration of Lie-Poisson Systems using the mid-point rule. Since such systems result from the reduction of hamiltonian systems with symmetry by Lie group actions, we also present examples of reconstruction rules for the full dynamics. A primary motivation is to preserve in the integration process, various conserved quantities of the original dynamics. A main result of this paper is an $O\left(h^3\right)$ error estimate for the Lie-Poisson structure where h is the integration step-size. We note that Lie-Poisson systems appear naturally in many areas of physical science and engineering, including theoretical mechanics of fluids and plasmas, satellite dynamics, and polarization dynamics. In the present paper we consider a series of progressively complicated examples related to rigid body systems. We also consider a dissipative example associated to a Lie-Poisson system. The behavior of the mid-point rule and an associated reconstruction rule is numerically explored.

[1] This work was supported in part by the AFSOR University Research Initiative Program under grants AFSOR-87-0073 and AFSOR-90-0105, by the National Science Foundation's Engineering Research Centers Program : NSFD CDR 8803012, by NSF Research Initiation Grant NSF BCS 8907722, and also by the Army Research Office through the Mathematical Sciences Institute at Cornell University.

[2] Assistant Professor, Department of Civil Engineering and Systems Research Center.

[3] Professor, Department of Electrical Engineering and Systems Research Center.

[4] Post Doctoral Scholar, Mathematics Department and Systems Research Center.

Table of Contents

Almost Poisson Integration of Rigid Body Systems

1 Introduction

Natural dynamical systems often display a variety of analytic and geometric structures in their mathematical descriptions. Associated to such structures, there are various conserved quantities or invariants of analytic as well as geometric character. For instance, in hamiltonian mechanics of particles in a central force field, one has conservation of energy and total angular momentum. The phase space volume is also conserved. The latter is an example of a geometric conserved quantity. In the case of dissipative systems the volume decays. In the study of such systems via computer simulation, it is very desirable to use computational schemes that admit the same set of invariants (or decay rates). More precisely, one would like to preserve underlying geometric structures and symmetries even in the discrete-time dynamics (computational scheme), in the interest of long-term predictions. If, as is customary, one were to use off-the-shelf schemes (e.g. fourth or higher order explicit Runge-Kutta [21], backward Euler, diagonally implicit Runge-Kutta [2]) to integrate the dynamics in such problems, then the computed trajectories show systematic deviations (decay or growth) in the quantities that are physically conserved. Thus, such numerical simulations are an unreliable guide to the long-term dynamic behavior. For related comparisons, see Channel and Scovel [6].

For some time, there has been steady interest in the design of algorithms that have the facility to closely mimic hamiltonian dynamics. In the work of the Beijing school [10,11], we find a systematic exploration of symplectic schemes (via generating functions) for classical hamiltonian systems on flat spaces. In particular, the mid-point rule plays a prominent role in that work, as explained below. In the present paper, we are concerned with systems that evolve on cotangent bundles of Lie groups, a basic example being the free rigid body with the rotation group as configuration space. If the hamiltonian is fully reducible by the group, as is the case in the rigid body example, then the dynamics drops to the flat space of linear functionals on the Lie algebra of the Lie Group, and hence the mid-point rule is well-defined globally in the reduced variables. The hamiltonian structure of the reduced equations is however noncanonical and is referred to as a `Lie-Poisson` structure. It is a principal goal of

this paper to explore the applications of the mid-point rule and related reconstruction rules to such Lie-Poisson equations via a series of progressively complicated examples. In general, the mid-point rule is not exactly Poisson structure preserving (and hence the terminology of almost Poisson integration). However, by a small miracle involving the Jacobi identity, the mid-point rule is indeed second order accurate in the Poisson structure and to this end we give an error formula.

The structure of the paper is as follows. In Section 2 we present the basic model of (noncanonical) Poisson dynamics and summarize some of its properties. We also specialize it to the classical canonical setting. In Section 3 we discuss the mid-point rule and present an error formula for the Poisson bracket. The mid-point rule is applied to a variety of examples in Section 4; these include rigid body dynamics, heavy top, dual spin problem, and dual spin with damping. A key result is the derivation of a reconstruction formula for elements in $SO(3)$ (the rotation group), which conserves spatial angular momenta. Sections 5 and 6 discuss issues in the numerical implementation of the proposed algorithms. Finally, numerical examples and simulation as well as animation results for rigid body systems are presented in Section 7.

We note in the previous work of Marsden and Ge-Zhong [13] a Lie-Poisson Hamilton-Jacobi theory has been developed. This theory leads to algorithms that preserve the Lie-Poisson structure exactly, but do not typically conserve the Hamiltonian. Recently, Simo and Wong [24] have used a Newmark-Based algorithm to study rigid body dynamics. When the parameters of their algorithms are set so that energy and momentum will be conserved, their algorithm reduces to the mid-point rule with an exponential map. We note, however, that the work of Simo and Wong does not consider errors from the viewpoint of conserving the Poisson structure, and has not been extended to applications with a general Lie-Poisson setting. For other earlier work on the midpoint rule we refer the reader to Elliot [8,9].

2 The Model

In the present paper we are concerned with hamiltonian models of the form,

$$\dot{z} = \Lambda(z)\nabla H\,(z)\,. \tag{1}$$

Here $\Lambda(z)$, the Poisson tensor, is an $n \times n$ skew-symmetric matrix for each z and H is the

hamiltonian. In addition, the tensor $\Lambda(z)$ satisfies a set of differential equations (Jacobi identity):

$$\sum_l \frac{\partial \Lambda^{ij}(z)}{\partial z_l}\Lambda^{lk}(z) + \frac{\partial \Lambda^{jk}(z)}{\partial z_l}\Lambda^{li}(z) + \frac{\partial \Lambda^{ki}(z)}{\partial z_l}\Lambda^{lj}(z) = 0. \tag{2}$$

With condition (2) the operation,

$$\{f, g\} = \nabla f^T \Lambda(z) \nabla g \tag{3}$$

is a well-defined Poisson bracket on the space of smooth functions on $\mathbb{R}^n$. It is remarkable that the equations of many physical and engineering problems are based on models of the form of (1) or perturbations thereof. We note, for example, the dynamics of dual spin satellites [17], accelerator dynamics [7], motion of a heavy top [3], Euler's elastica [20], and dynamics of rods, plates and shells [23]. Also see Simo, Marsden and Krishnaprasad [23] for infinite-dimensional examples, and Marsden et al. [19] for a general discussion.

The dynamics (1) can be re-expressed in terms of the Poisson bracket (3) as

$$\dot{z}_i \;=\; \{z_i,\; H\}. \tag{4}$$

When $\Lambda(z)$ is linear in z, the bracket structure is said to be *of Lie-Poisson type.* Several of the earlier mentioned examples are of this variety. In this case one sets,

$$\Lambda^{ij}(z) = \sum_{k=1}^{n} \Gamma_{ij}^k z_k \tag{5}$$

where $\Gamma_{ij}^k = -\Gamma_{ji}^k$ and the Jacobi identity (2) takes the form,

$$\sum_{l=1}^{n} \Gamma_{ij}^l \Gamma_{lk}^r + \Gamma_{jk}^l \Gamma_{li}^r + \Gamma_{ki}^l \Gamma_{lj}^r = 0, \quad 1 \;\leq\; i, j, k \;\leq\; n. \tag{6}$$

It is further well-known that in this case the underlying vector space $\mathbb{R}^n$ can be given the structure of a Lie algebra [27] with the structure constants Γ_{ij}^k in a suitable basis. Now let $\Phi : \mathbb{R}^n \to \mathbb{R}^n$ be a diffeomorphism. Φ is said to be a Poisson automorphism if it preserves the Poisson structure, i.e. for smooth functions f, g,

$$\{\; f,\; g\;\} \circ \Phi \;=\; \{\; f \circ \Phi,\; g \circ \Phi\;\},$$

or alternatively its Fréchet derivative satisfies,

$$(D\Phi(z))\Lambda(z)(D\Phi(z))^T = \Lambda(\Phi(z)). \tag{7}$$

Here the superscript T denotes matrix transpose. We recall the well-known result(see Weinstein [27]),

Proposition 1 : The flow Φ^t of the system (1) satisfies:

(a) It is a Poisson automorphism $\forall\ t$.

(b) $H(\Phi^t(z)) = H(z)$.

(c) If $C : \mathbb{R}^n \to \mathbb{R}$ is a function such that

$$\Lambda(z)\nabla C(z) = 0,$$

then C yields a kinematic conservation law of (1).

Remark 1: Functions C as in Proposition (1) are called *Casimir functions.* For canonical hamiltonian systems,

$$\Lambda(z) = \begin{bmatrix} 0 & \mathbb{1} \\ -\mathbb{1} & 0 \end{bmatrix}.$$

Here $\mathbb{1}$ denotes the identity transformation on $\mathbb{R}^m$, where $m = n/2$. The corresponding canonical Poisson bracket is given by the well-known formula [12]

$$\{f,\ g\} = \sum_{i=1}^{m} \left[\frac{\partial f}{\partial q_i} \frac{\partial g}{\partial p_i} - \frac{\partial f}{\partial p_i} \frac{\partial g}{\partial q_i} \right] \tag{8}$$

where the position coordinates q_i and conjagate momenta p_i are given by

$$z = (q_1, \cdots,\ q_m,\ p_1, \cdots, p_m)^T \qquad \text{with } n = 2m.$$

For canonical hamiltonian systems, Casimir functions are constants. However, in the Lie-Poisson setting, nontrivial Casimir functions are common, as will be demonstrated by our examples in Section 4.

3 The Mid-point Rule

A basic concern of this paper is to investigate numerical algorithms that closely mimic Proposition (1). In particular, we are interested in the mid-point rule, a scheme well-known to be symplectic in the canonical case [11]. Consider the implicit recursion,

$$\left[\frac{z^{k+1}-z^k}{h}\right] = \Lambda\left(\frac{z^k+z^{k+1}}{2}\right)\nabla H\left(\frac{z^k+z^{k+1}}{2}\right). \tag{9}$$

This is a discrete analog of (1) for time-step h. It is a second order accurate integrator, and for small enough h, defines a diffeomorphism, Φ_H^h via,

$$z^{k+1} = \Phi_H^h\left(z^k\right). \tag{10}$$

We compute the Fréchet derivative $D\Phi_H^h\,(z)$ as follows. By definition, $y = \Phi_H^h\,(z)$ is the unique solution to the implicit equation,

$$\begin{aligned} F(z,y) &\stackrel{\triangle}{=} y - z - h\Lambda(\frac{z+y}{2})\,\nabla H\left(\frac{z+y}{2}\right) \\ &= 0. \end{aligned} \tag{11}$$

Differentiating $F\left(z,\ \Phi_H^h\,(z)\right) = 0$, we get,

$$D_1F + D_2\,F \circ D\,\Phi_H^h = 0, \tag{12}$$

where $D_i\,F$, $i = 1,2$ denote the partial Fréchet derivatives. For h small enough, D_2F has an inverse, and (12) may be rearranged to give,

$$D\Phi_H^h\,(z) = -\,(D_2F)^{-1}\cdot(D_1F). \tag{13}$$

For the special case $\Lambda(z) \equiv \Lambda$ a constant, it is easy to see that,

$$\begin{aligned} D_1F &= -\mathbb{1} - \frac{h}{2}\Lambda H_{zz}\left(\frac{z+\Phi_H^h\,(z)}{2}\right), \\ \text{and} \qquad D_2F &= \mathbb{1} - \frac{h}{2}\Lambda H_{zz}\left(\frac{z+\Phi_H^h\,(z)}{2}\right). \end{aligned}$$

Letting $Q(z) = H_{zz}\left(\frac{z + \Phi_H^h(z)}{2}\right)$ denote the symmetric Hessian matrix, we get

$$D\Phi_H^h(z) = \left[\mathbb{1} - \frac{h}{2}\Lambda Q(z)\right]^{-1}\left[\mathbb{1} + \frac{h}{2}\Lambda Q(z)\right]. \tag{14}$$

Proposition 2: (Wang Dao Liu [26]). If $\Lambda(z) \equiv \Lambda$ a constant, then the mid-point rule is a Poisson automorphism.

Proof: We need to show that,

$$D\Phi_H^h(z)\Lambda(D\Phi_H^h(z))^T = \Lambda.$$

Based on the above calculations, this reduces to showing that,

$$\left[(\mathbb{1} - \frac{h}{2}\Lambda Q(z))^{-1}(\mathbb{1} + \frac{h}{2}\Lambda Q(z))\right]\Lambda\left[(\mathbb{1} - \frac{h}{2}\Lambda Q(z))^{-1}(\mathbb{1} + \frac{h}{2}\Lambda Q(z))\right]^T$$
$$= \Lambda.$$

which is equivalent to showing that

$$\left[\mathbb{1} + \frac{h}{2}\Lambda Q(z)\right]\Lambda\left[\mathbb{1} + \frac{h}{2}\Lambda Q(z)\right]^T = \left[\mathbb{1} - \frac{h}{2}\Lambda Q(z)\right]\Lambda\left[\mathbb{1} - \frac{h}{2}\Lambda Q(z)\right]^T.$$

This follows from the fact that $\Lambda = -\Lambda^T$ and $Q(z) = Q(z)^T$. The proof is now complete.

Remark 2: It follows from the above proposition that, if $\Lambda(z) \equiv \Lambda = \begin{pmatrix} 0 & \mathbb{1} \\ -\mathbb{1} & 0 \end{pmatrix}$, i.e. we are in the canonical case, then the mid-point rule preserves the classical Poisson bracket (8). Thus we recover the well-known result that the mid-point rule is a symplectic integrator (Feng Kang [11]). This result also follows from the observation that in the canonical case, formula (14) becomes a Cayley transform of an infinitesimally symplectic matrix $\Lambda Q(z)$ and hence $D\Phi_H^h(z)$ is symplectic.

When $\Lambda(z)$ is not a constant, in general, the mid-point rule is not a Poisson automorphism. However, if $\Lambda(z)$ is linear in z - i.e. we are in the Lie-Poisson setting - then the following theorem shows that the mid-point rule is an `almost` Poisson integrator in the

sense that it preserves the Lie-Poisson structure up to second order. To this end, an error formula is given.

Theorem 1: For Lie-Poisson systems the mid-point rule is almost a Poisson automorphism. We have the error formula,

$$\begin{aligned} D\Phi_H^h(z)\Lambda(z)(D\Phi_H^h(z))^T \; - \; \Lambda(\Phi_H^h(z)) \\ = \; - \; \frac{h^3}{4} K(z)\Lambda\left(\Lambda(\frac{z \; + \; \Phi_H^h(z)}{2})w\right) K(z)^T \; + \; O(h^4) \end{aligned} \tag{15}$$

where

$$\begin{aligned} K(z) &= \Lambda(\frac{z \; + \; \Phi_H^h(z)}{2})Q \; + \; \Omega(w), \\ Q &= D^2H(\frac{z \; + \; \Phi_H^h(z)}{2}), \\ w &= \nabla H(\frac{z \; + \; \Phi_H^h(z)}{2}). \end{aligned}$$

Here Q is the Hessian of H evaluated at the mid-point, and Ω is defined by requiring that $\Omega(v)y \; = \; \Lambda(y)v$, where $v, y \epsilon \, \mathbb{R}^n$.

Proof: First note that, from the definitions for partial Fréchet derivatives, for $v \epsilon \, \mathbb{R}^n$,

$$\begin{aligned} D_1F(z, \; y)v \; \underline{\triangle} \; \lim_{t \downarrow 0} \; \frac{F(z \; + \; tv, \; y) \; - \; F \; (z, \; y)}{t} \\ D_2F(z, \; y)v \; \underline{\triangle} \; \lim_{t \downarrow 0} \; \frac{F(z, \; y \; + \; tv) \; - \; F(z, \; y)}{t} \end{aligned}$$

and it can be verified that,

$$D_1F = \; - \; \left[\mathbb{1} \; + \; \frac{h}{2}\Lambda(\frac{z \; + \; y}{2})D^2H(\frac{z \; + \; y}{2}) \; + \; \frac{h}{2} \; \Omega(\nabla H(\frac{z \; + \; y}{2}))\right] \tag{16}$$

and

$$D_2F = \; \left[\mathbb{1} \; - \; \frac{h}{2}\Lambda(\frac{z \; + \; y}{2}) \; D^2H(\frac{z \; + \; y}{2}) \; - \; \frac{h}{2}\Omega(\nabla H(\frac{z \; + \; y}{2}))\right]. \tag{17}$$

In the following derivation, y in (16) and (17) will be used to denote $\Phi_H^h(z)$. The error in the Poisson structure Λ due to discrete time stepping by Φ_H^h is given by,

$$\varepsilon \;=\; D\Phi_H^h\;(z)\;\Lambda\;(z)\;(D\Phi_H^h(z))^T \;-\; \Lambda\;(\Phi_H^h(z)).$$

Substituting (13), (16), and (17) gives,

$$\varepsilon \;=\; (D_2\;F)^{-1}\;(\varepsilon_1)\;(D_2\;F)^{T\;-1} \tag{19}$$

where,

$$\varepsilon_1 \;=\; (D_1\;F)\;\Lambda\;(z)\;(D_1\;F)^T \;-\; (D_2\;F)\;\Lambda\;(y)\;(D_2\;F)^T. \tag{20}$$

Since $(D_2\;F)^{-1} \;=\; \mathbb{1} + O(h)$, we are mainly interested in the behavior of ε_1 as a function of h. For convenience, let us denote the midpoint $(z \;+\; \Phi_H^h\;(z))/2$ as x. In formula (20), multiplying out the terms, invoking (16), (17) and the linearity of Λ and Ω in their respective arguments, we get,

$$\begin{aligned}
\varepsilon_1 \;=\; & \left[-\;\Lambda(\delta) \;+\; h\Omega(w)\Lambda(x) \;+\; h\;\Lambda(x)\Omega(w)^T\right] \\
& +\; \left[h\Lambda(x)Q\;\Lambda \;+\; h\;\Lambda(x)Q\;\Lambda(x)^T\right] \\
& +\; \left[-\;\frac{h^2}{4}\;\Lambda(x)Q\;\Lambda(\delta)Q\Lambda(x)^T \;-\; \frac{h^2}{4}\Omega(w)\Lambda(\delta)Q\Lambda(x)^T\right] \\
& -\; \left[\frac{h^2}{4}\;\Lambda(x)Q\Lambda(\delta)\Omega(w)^T \;+\; \frac{h^2}{4}\Omega(w)\Lambda(\delta)\Omega(w)^T\right]
\end{aligned} \tag{21}$$

Here $\delta \;=\; y \;-\; z \;=\; \Phi_H^h\;(z) \;-\; z$. The second square bracket in ε_1 vanishes because $\Lambda \;=\; -\;\Lambda^T$. Recall from (9) that,

$$\delta \;=\; h\Lambda(x)w. \tag{22}$$

Substituting from (22) in (21) the first square bracket in (21) is linear in h, and when multiplied by v takes the form,

$$h\left[-\Lambda(\Lambda(x)w) \;+\; \Omega(w)\;\Lambda(x) \;+\; \Lambda(x)\Omega(w)^T\right]v. \tag{23}$$

We wish to show that the expression (23) also vanishes. Note that this is equivalent to showing that

$$\left[-\Lambda(\Lambda(x)w) \;+\; \Omega(w)\;\Lambda(x) \;+\; \Lambda(x)\Omega(w)^T\right]v = \;0, \qquad \forall\; v \;\epsilon\; \mathbb{R}^n. \tag{24}$$

Recalling that the definition for Ω is given by $\Omega(v)y \;=\; \Lambda(y)v$, the left hand side of (24) can be re-written as,

$$-\;\Omega(v)\Lambda\;(x)w + \;\Omega(w)\;\Omega(v)x + \;\Lambda(x)\;\Omega(w)^T\,v. \tag{25}$$

Expanding Ω and Λ via the structure constants Γ_{ij}^k, one can show that precisely because of the Jacobi identity (6), the expression (25) vanishes for all $v,\; w,\; x \quad \epsilon\, \mathbb{R}^n$. This is the small miracle alluded to in the Introduction! Collecting together the terms in the third square bracket in formula (21) for ε_1 we get,

$$\begin{aligned}
\varepsilon_1 \;&=\; -\;\frac{h^3}{4}\;\left[\Lambda(x)\;Q \;+\; \Omega(w)\right]\;\Lambda\;\left(\Lambda(x)w\right)\;\left[\Lambda(x)\;Q \;+\; \Omega(w)\right]^T \\
&=\; -\;\frac{h^3}{4}\;K(z)\;\Lambda\;\left[\Lambda(\frac{z \;+\; \Phi_H^h(z)}{2})w\right]\;K(z)^T.
\end{aligned}$$

It follows that

$$\begin{aligned}
\varepsilon =&\; \left(D_2\;F\right)^{-1}\;\left(\varepsilon_1\right)\left(D_2\;F\right)^{T-1} \\
=&\; \left(\mathbb{1} \;+\; O(h)\right)^{-1}\;\left(\varepsilon_1\right)\left(\mathbb{1} \;+\; O(h)\right)^{-1} \\
=&\; -\frac{h^3}{4}\;K(z)\Lambda\left(\Lambda(\frac{z \;+\; \Phi_H^h(z)}{2})w\right)\;K(z)^T \;+\; O(h^4)
\end{aligned}$$

This completes the proof.

Conserved Quantities of Poisson System (1): It is well-known fact that mid-point rule is a second order algorithm. Accordingly, a conserved quantity is expected to be

approximated accurately up to second order. In fact, letting F be a first integral of (1), we have

$$\nabla F(z)^T \Lambda(z) \nabla H(z) \;=\; 0, \qquad \forall\, z \in \mathbb{R}^n. \tag{26.1}$$

Assuming F is three times continuously differentiable, by Taylor's theorem we can expand F around z^k as

$$\begin{aligned} F(z^{k+1}) \;&= F(z^k) + \nabla F(z^k)^T (z^{k+1} - z^k) + \frac{1}{2} D^2 F(z^k) \cdot (z^{k+1} - z^k) \cdot (z^{k+1} - z^k) \\ &\quad + \frac{1}{6} D^3 F(z^k) \cdot (z^{k+1} - z^k) \cdot (z^{k+1} - z^k) \cdot (z^{k+1} - z^k) + O(\|z^{k+1} - z^k\|^4). \end{aligned} \tag{26.2}$$

Substituting the mid-point rule (9) in (25.3), it can be checked that

$$F(z^{k+1}) - F(z^k) \;=\; \frac{1}{24} D^3 F(z^k) \cdot u \cdot u \cdot u + O(h^4), \tag{26.3}$$

where

$$u \;=\; \Lambda\left(\frac{z^{k+1} + z^k}{2}\right) \nabla H\left(\frac{z^{k+1} + z^k}{2}\right).$$

Equation (26.3) is an error formula for conserved quantities of (1), which contains only third or higher order terms. It follows that the mid-point rule (9) preserves exactly any conserved quantity having only linear and quadratic terms, including Casimir functions and the Hamiltonian for (1). As a consequence, we have the following Proposition which will be referred to later.

Proposition 3: The discrete analog (9) conserves all Casimir functions and the Hamiltonian H of (1) if they contain only linear and quadratic terms.

In the next section, we consider a set of examples related to rigid body mechanics that captures the essence of the results of this section.

4. Examples from Rigid Body Mechanics

The noncanonical hamiltonian model of this paper - in particular the Lie-Poisson case - arises naturally in a variety of problems in rigid body mechanics. In this section, we discuss: (a) the simple rigid body, (b) the heavy top, (c) dual spin satellite, and (d) dual-spin with damping.

4.1 Simple Rigid Body Spinning Freely in Space

Recall that the equations of motion for a simple rigid body in three dimensions take the form:

$$\dot{A} = A\widehat{\Omega} \qquad \text{where} \qquad A \in SO(3) \tag{27}$$

$$I\dot{\Omega} = I\Omega \times \Omega. \tag{28}$$

Here, $A \in SO(3)$ the group of 3×3 rotation matrices, is the matrix of direction cosines for a body frame attached to the rigid body as viewed in an inertial frame; see Figure [1]. The vector Ω is the body angular velocity of the rigid body and $\widehat{\Omega}$ represents a skew-symmetric matrix:

$$\widehat{\Omega} = \begin{bmatrix} 0 & -\Omega_3 & \Omega_2 \\ \Omega_3 & 0 & -\Omega_1 \\ -\Omega_2 & \Omega_1 & 0 \end{bmatrix}$$

The symbol $\times$ denotes the cross-product in $\mathbb{R}^3$. Notice that for an arbitrary vector y, $\widehat{\Omega}y = \Omega \times y$. The matrix I denotes the moment of inertia tensor of the rigid body in the body frame. If $m = I\Omega$ denotes the body angular momemtum, then we can re-write (27) and (28) as:

$$\dot{A} = A\widehat{I^{-1}m} \tag{29}$$

$$\dot{m} = \widehat{m}I^{-1}m. \tag{30}$$

Several observations are in order:

[a] Equation (30) is the reduction of the full dynamics (justified by the $SO(3)$-invariance of the kinetic energy), [1].

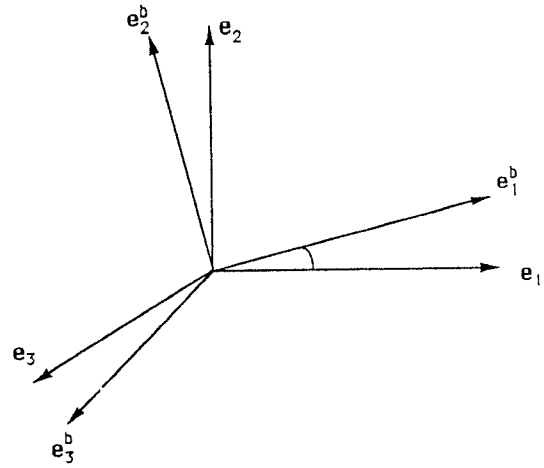

Figure [1] : Configuration of Inertial and Body Frames

[b] Equation (30) is Lie-Poisson in the sense of Section 2 with Poisson tensor $\Lambda(m) = \widehat{m}$ and hamiltonian $H(m) = \frac{1}{2} m \cdot I^{-1} m$. Hereafter $\cdot$ denotes the dot product.

[c] $C(m) = \frac{1}{2}\|m\|^2$ is a Casimir function associated to (29). It is a quadratic conserved quantity.

It follows that if we can integrate (30), then the kinematic variable A can be reconstructed by quadrature of (29). This process can be mimicked in discrete algorithms also. In particular, one might integrate (30) numerically via the mid-point rule (thereby conserving H and C, see Proposition 2) and then *devise a reconstruction rule for updating the attitude matrix in such a way that spatial angular momentum $\pi = Am$ is also conserved.*

4.1.1 Discrete Update in Body Momentum

A two-step process is employed to compute the discrete update in body momentum and spatial attitude. First, let m_k and m_{k+1} be the body momentum at timesteps h_k and h_{k+1}, respectively, and $h = h_{k+1} - h_k$. The discrete update in body momentum corresponds to the mid-point rule applied to (30), i.e.:

$$\frac{m_{k+1} - m_k}{h} = \left[\frac{m_k + m_{k+1}}{2}\right] \times I^{-1} \left[\frac{m_k + m_{k+1}}{2}\right] \tag{31}$$

Equations (31) are solved by iteration for the discrete update in body momentum m_k to m_{k+1}. It follows from Proposition 3 that this update scheme conserves both $H(m)$ and $C(m)$.

4.1.2 Discrete Update in Spatial Attitude (reconstruction rule)

Once equations (30) are solved, our reconstruction rule for the update in spatial attitude is given by the explicit set of equations:

$$A_{k+1} = A_k \left[\mathbb{1} - \widehat{b_k}\right]^{-1} \left[\mathbb{1} + \widehat{b_k}\right] \tag{32.1}$$

$$\text{where} \qquad b_k = \left[\frac{h}{2}\right] I^{-1} \left[\frac{m_k + m_{k+1}}{2}\right]. \tag{32.2}$$

The explicit recursion (32) - Cayley Transform for $SO(3)$ - is arrived at by requiring conservation of spatial angular momentum $\pi = Am$,

$$\pi_{k+1} = \pi_k = A_{k+1} m_{k+1} = A_k m_k. \tag{33.1}$$

This suggests a suitable form for the update is

$$A_{k+1} = A_k A_1 = A_k \left[\mathbb{1} - \widehat{b_k}\right]^{-1} \left[\mathbb{1} + \widehat{b_k}\right], \tag{33.2}$$

where $\widehat{b_k}$ is skew-symmetric and needs to be determined so that (33.2) closely approximates the matrix exponential implied by $\dot{A} = A\widehat{\Omega}$. Substituting (33.2) into (33.1) and rearranging terms gives

$$\widehat{[m_k + m_{k+1}]} b_k = [m_{k+1} - m_k]. \tag{33.3}$$

Notice that if $\widehat{[m_k + m_{k+1}]} b_k = [m_{k+1} - m_k]$ has a solution, then, by the Fredholm alternative theorem,

$$(m_{k+1} - m_k) \perp \quad \text{kernel} \quad \widehat{[m_{k+1} + m_k]}^T \tag{33.4}$$

$$= \text{kernel} \quad \widehat{[m_{k+1} + m_k]} \tag{33.5}$$

$$= \{\alpha \, [m_{k+1} + m_k] \quad | \quad \alpha \epsilon \, \mathbb{R}\}. \tag{33.6}$$

This implies $[m_k + m_{k+1}] \cdot [m_{k+1} - m_k] = 0$, and thus conservation of Casimir is a necessary condition for conservation of spatial angular momentum. The general solution to (33.3) is given by

$$b_k = \lambda_k \cdot [m_{k+1} - m_k] \times [m_{k+1} + m_k] + \alpha_k [m_{k+1} + m_k]. \tag{34}$$

How do we choose λ_k and α_k ? First, note:

$$\begin{aligned}
[m_{k+1} - m_k] &= [m_k \widehat{+} m_{k+1}] b_k && (35.1)\\
&= [m_k + m_{k+1}] \times b_k && (35.2)\\
&= [m_k + m_{k+1}] \times \lambda_k \left([m_{k+1} - m_k] \times [m_{k+1} + m_k] \right) \quad + \\
&\quad [m_k + m_{k+1}] \times \alpha_k [m_{k+1} + m_k] && (35.3)\\
&= [m_k + m_{k+1}] \times \lambda_k [m_{k+1} - m_k] \times [m_{k+1} + m_k] && (35.4)\\
&= \|m_k + m_{k+1}\|^2 \cdot \lambda_k \cdot [m_{k+1} - m_k]. && (35.5)
\end{aligned}$$

This implies

$$\lambda_k = \frac{1}{\|m_k + m_{k+1}\|^2}. \tag{36}$$

To get $\alpha_k \neq 0$, the discrete update for body momentum is substituted into (34). Rearranging terms and selecting

$$\alpha_k = \left[\frac{h}{4}\right] \cdot \frac{[m_k + m_{k+1}] \cdot I^{-1} [m_k + m_{k+1}]}{\|m_k + m_{k+1}\|^2} \tag{37.1}$$

gives

$$b_k = \left[\frac{h}{2}\right] I^{-1} \left[\frac{m_k + m_{k+1}}{2}\right]. \tag{37.2}$$

Remark 3: Table [1] summarizes the discrete equations for Rigid Body. Notice that the matrix product

$$\left[\mathbb{1} - \widehat{b_k}\right]^{-1} \left[\mathbb{1} + \widehat{b_k}\right] = \exp\left[h I^{-1} \left(\widehat{\frac{m_k + m_{k+1}}{2}} \right) \right] + O(h^3) \tag{38.1}$$

In fact, if $I^{-1}m$ in (29) is a constant vector across the timestep, then the incremental rule for the attitude matrix becomes

$$A_{k+1} \;=\; A_k \,\exp(h\widehat{I^{-1}m}). \tag{38.2}$$

Thus, the update rule (33.2) can be intuitively thought of as the composition of two steps. First, the angular momentum in (29) is approximated by an intermediate value. Second, the exponential in (38.2) is approximated in terms of b_k by the formula (38.1). We summarize our energy-momentum preserving algorithm for a simple rigid body spinning freely in space as follows.

Update for Body Momentum:

$$\frac{m_{k+1}-m_k}{h} = \left[\frac{m_k+m_{k+1}}{2}\right] \times I^{-1}\left[\frac{m_k+m_{k+1}}{2}\right]$$

Update for Spatial Attitude:

$$A_{k+1} = A_k\left[\mathbb{1}-\widehat{b_k}\right]^{-1}\left[\mathbb{1}+\widehat{b_k}\right]$$

$$\text{where} \qquad b_k = \left[\frac{h}{2}\right] I^{-1}\left[\frac{m_k+m_{k+1}}{2}\right]$$

Table [1] : Discrete Equations for Rigid Body

4.2 Heavy Top

Consider the motion of a rigid body fixed at a stationary point subject to the action of a uniform gravitational field, as shown in Figure 2.

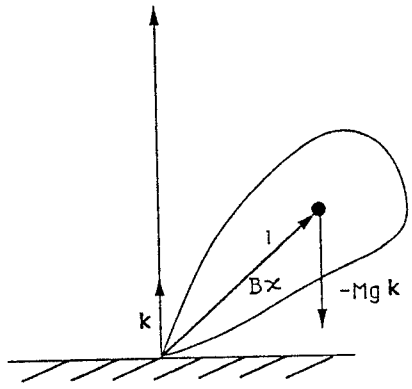

Figure [2] : Diagram for Heavy Top

If the body frame is fixed at a point O, then we define the unit vector from O to the center of mass in the body frame as χ. The spatial inertial frame is also at O with the vector $\mathbf{k}$ being one of its axis. Notice that the body is acted on by a gravitational force $-Mg\mathbf{k}$, where M is the mass of the rigid body, and g is the constant of acceleration due to gravity.

The kinematics of the body frame relative to the interial frame are governed by

$$\dot{A} = A\widehat{\Omega} \qquad \text{where} \qquad A \in SO(3). \tag{39}$$

Moreover, if $v = A^T \cdot \mathbf{k}$, then the equations of motion for the heavy top can be expressed as

$$\dot{m} = m \times I^{-1}m + Mglv \times \chi \tag{40}$$

$$\dot{v} = v \times I^{-1}m \tag{41}$$

where $m = I\Omega$ is body momentum, l the distance between O and the body center of mass, and I the moment of inertia of the heavy top relative to the body frame. In addition, we note:

[a] Equations (40) and (41) are Lie-Poisson in the sense of Section 2 with Poisson tensor

$$\Lambda(m) = \begin{bmatrix} \widehat{m} & \widehat{v} \\ \widehat{v} & 0 \end{bmatrix}$$

and total energy

$$H(m, v) = \frac{1}{2} m \cdot I^{-1} m + Mglv \cdot \chi. \tag{42}$$

See Marsden, Ratiu and Weinstein [18] for details.

[b] The heavy top problem has two Casimirs:

$$C_1(m, v) = \frac{1}{2}\|v\|^2 \tag{43}$$

$$C_2(m, v) = m \cdot v. \tag{44}$$

Equation (43) reflects the fact that $A \in SO(3)$, and equation (44) says that spatial angular momentum along the vertical axis $\mathbf{k}$ passing through O is conserved.

4.2.1 Discrete Update for Heavy Top

The corresponding discrete equations of motion using mid-point rule are

$$\frac{m_{k+1} - m_k}{h} = \left[\frac{m_k + m_{k+1}}{2}\right] \times I^{-1} \frac{m_k + m_{k+1}}{2} + Mgl \frac{v_k + v_{k+1}}{2} \times \chi \tag{45.1}$$

$$\frac{v_{k+1} - v_k}{h} = \left[\frac{v_k + v_{k+1}}{2}\right] \times I^{-1} \frac{m_k + m_{k+1}}{2}. \tag{45.2}$$

As noted in Proposition 3, the mid-point rule preserves exactly the Hamiltonian and Casimirs which contain only linear and quadratic terms. The above scheme (45) conserves both Casimir functions C_1, C_2 in (43), (44) and the Hamiltonian in (42).

4.2.2 Discrete Update in Spatial Attitude

After equations (45) are solved, the discrete update and spatial attitude of the heavy top is given by the equation

$$A_{k+1} = A_k \left[\mathbb{1} - \widehat{b_k}\right]^{-1} \left[\mathbb{1} + \widehat{b_k}\right] \tag{46.1}$$

$$\text{where} \qquad b_k = \left[\frac{h}{2}\right] I^{-1} \left[\frac{m_k + m_{k+1}}{2}\right]. \tag{46.2}$$

The justification of the reconstruction rule (44) is analogous to the one used for the simple rigid body.

4.3 Dual Spin Satellite

Dual spin satellites consist of a simple rotating platform carrying one or more symmetric rotors spinning at constant rates about an axis fixed relative to the platform. The purpose of the rotors is to exert internal reaction torques on the platform. Assuming there are no external forces acting on the system, the net effect is a transfer of internal momentum from the platform to the rotors. In the presence of a suitable damping mechanism and sufficiently high rotor velocities, the spacecraft angular velocity will align itself with the rotor axis.

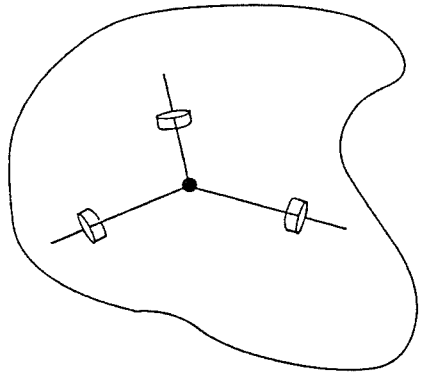

Figure [3] : Schematic of Dual Spin Satellite

For the purposes of this study we are interested only in dual spin satellites where the axis of the rotors passes through the center of mass of the platform with fixed rotors. The attitude kinematics of the satellite relative to an inertial frame is given by

$$\dot{A} = A\widehat{\Omega} \qquad \text{where} \qquad A \in SO(3). \tag{47}$$

The equation of motion for body angular momentum is now,

$$\dot{m} = (\widehat{m + l}) \cdot \nabla_m H(m) \tag{48.1}$$

$$= [m + l] \times I^{-1} m \tag{48.2}$$

where m is a vector of body angular momentum, and I is the locked moment of inertia tensor of the body plus rotor system. The satellite has an internal rotor spinning at constant relative angular momentum l. We also note:

[a] Equations (48) are Lie-Poisson in $\mathbb{R}^3$ with Poisson tensor $\Lambda(m) = \widehat{m} + \widehat{l}$, and hamiltonian $H(m) = \frac{1}{2} m \cdot I^{-1} m$. See Krishnaprasad [17] for details.

[b] The dual spin satellite has one Casimir $C(m) = \|m + l\|^2$.

[c] The spatial angular momentum is $\pi = A(m + l)$, and is conserved since the torques generated by the rotors are internal torques.

4.3.1 Discrete Update in Body Momentum

The discrete update in body momentum is given by the midpoint rule:

$$\frac{m_{k+1} - m_k}{h} = \left[\frac{m_k + m_{k+1}}{2} + l\right] \times I^{-1}\left[\frac{m_k + m_{k+1}}{2}\right] \tag{49}$$

4.3.2 Discrete Update in Spatial Attitude

The discrete update in spatial attitude is

$$A_{k+1} = A_k \left[\mathbb{1} - \widehat{b_k}\right]^{-1} \left[\mathbb{1} + \widehat{b_k}\right] \tag{50.1}$$

$$\text{where} \qquad b_k = \left[\frac{h}{2}\right] I^{-1}\left[\frac{m_k + m_{k+1}}{2}\right]. \tag{50.2}$$

Remark 5: Following the steps in Section 4.1 it is easy to verify that the attitude update is momentum conserving. Indeed, techniques for reorienting the attitude of a satellite depend on a mechanism for transfering the balance of internal rotor and platform momenta, without affecting spatial angular momentum. Independently, by Proposition 3, the energy H and Casimir C are conserved by the momentum update (49).

4.4 Dual Spin Satellite with Damped Rotors

Dual spin satellites consist of a rigid body platform and several internal rotors. When the platform is fully operational, the rotors are set to spin at a constant angular velocity relative to the platform. Damping rotors act as dissipators of energy. Indeed, even in the

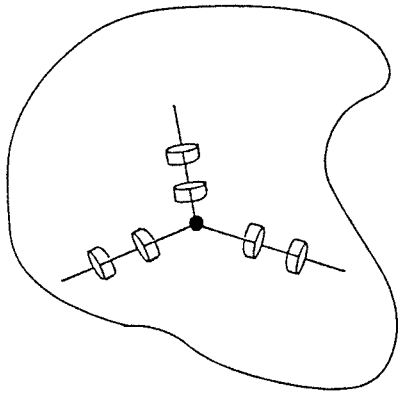

Figure [4] : Schematic of Dual Spin Satellite with Damping

presence of mild disturbances, the transfer of momentum from the platform to the damping rotors will result in a mechanism for attitude aquisition of the platform.

The equations of motion for a dual spin satellite with damping are composed of two parts. As with the two previous applications, the kinematics are given by

$$\dot{A} = A\widehat{\Omega} \qquad \text{where} \qquad A \in SO(3). \tag{51}$$

Let the diagonal matrix $\alpha = diag\,(\alpha_1, \alpha_2, \alpha_3)$, where $\alpha_i > 0$, and let $I_d = diag\,\left(I_d^1, I_d^2, I_d^3\right)$ be a diagonal matrix of moments of inertia of the damping rotors with respect to their spin axes. Note that $I_d^i \geq 0 \quad \text{for i} = 1, 2, 3$. Moreover, if m and l are as previously defined, and d a momentum vector associated to damping rotors, then the evolution of body angular momentum is governed by the equations

$$\dot{m} = (m + l + d) \times I^{-1} m - \gamma m + \delta d \tag{52.1}$$

$$\dot{d} = \gamma m - \delta d \tag{52.2}$$

where $\gamma = \alpha I^{-1}$ and $\delta = \alpha I_d^{-1}$, respectively. Although the system is not a hamiltonian system in the form of (1), we still have the following properties (see Krishnaprasad [17] for details):

[a] This system has one conserved quantity $C\,(m, d) = \|m + l + d\|^2$.

[b] The Lyapunov function for dual spin with damping is:

$$V(m,d) = \frac{1}{2} m \cdot I^{-1} m + \frac{1}{2} d \cdot {I_d}^{-1} d \tag{53.1}$$

It is decrescent with

$$\dot{V} \;=\; -({I_d}^{-1} d - I^{-1} m)^T \, \alpha ({I_d}^{-1} d - I^{-1} m), \tag{53.2}$$

along trajectories of (52). Again, see Krishnaprasad [17] for details.

[c] The spatial angular momentum $\pi = A\,[m + l + d]$ is also a conserved quantity.

4.4.1 Discrete Update in Body Momentum

The update in body momentum is given by the mid-point rule

$$\begin{aligned} \frac{m_{k+1} - m_k}{h} &= \left[\frac{m_k + m_{k+1}}{2} + l + \frac{d_k + d_{k+1}}{2}\right] \times I^{-1} \left[\frac{m_k + m_{k+1}}{2}\right] \\ &\quad - \gamma \left[\frac{m_k + m_{k+1}}{2}\right] + \delta \left[\frac{d_k + d_{k+1}}{2}\right] \qquad (54.1) \\ \frac{d_{k+1} - d_k}{h} &= \gamma \left[\frac{m_k + m_{k+1}}{2}\right] - \delta \left[\frac{d_k + d_{k+1}}{2}\right]. \qquad (54.2) \end{aligned}$$

4.4.2 Discrete Update in Spatial Attitude

The discrete update for spatial attitude is:

$$A_{k+1} = A_k \left[\mathbb{1} - \widehat{b_k}\right]^{-1} \left[\mathbb{1} + \widehat{b_k}\right] \tag{55.1}$$

$$\text{where} \qquad b_k = \left[\frac{h}{2}\right] I^{-1} \left[\frac{m_k + m_{k+1}}{2}\right]. \tag{55.2}$$

4.4.3 Conservation Law for Dual Spin with Damping

The system (52) admits C and π as conserved quantities. The Lyapunov function V decreases at a rate quadratic in the damping vector d. The discrete scheme (54)-(55) mimics these features, as one might expect. We leave it to the reader to verify that the discrete version of (53.2) is satisfied.

5.1 Numerical Integration Schemes

The solution procedure for each of the applications described in Sections (4.1) through to (4.4) is: (a) solve the implicit equations for the body momentum at timestep t_{k+1}, (b) solve the explicit equations for the update in spatial attitude.

5.1.1 Solution of Implicit Equations for Update in Body Momentum

Equations (31), (45), (49) and (54) are a systems of nonlinear ordinary differential equations (in vector form) that must be solved at each timestep for m_{k+1}.

First, each equation is written in component form and rearranged so that solving the problem is equivalent to finding the root of an equation. This gives 6 equations for dual spin with damping and heavy top applications, and 3 equations for rigid body and dual spin. Equations (58) in Table [2] show, for example, the 3 component equations of body momentum for the dual spin problem. The adopted notation for m, l or I is timestep i of component j in the $[i,j]$ subscript brackets.

A damped Newton-Raphson procedure is used to solve the component equations at each timestep. If m^p_{k+1} is the p^{th} iterate of body momentum at timestep $k+1$, then the equations to be solved at each iterate are obtained by expanding $g_1(m_k, m^p_{k+1})$, $g_2(m_k, m^p_{k+1})$ and $g_3(m_k, m^p_{k+1})$ in a Taylor series about m^p_{k+1}, truncating all second order terms and higher terms, and solving the set of equations:

$$\begin{bmatrix} \frac{\partial g_1}{\partial m^p_{[k+1,1]}} & \frac{\partial g_1}{\partial m^p_{[k+1,2]}} & \frac{\partial g_1}{\partial m^p_{[k+1,3]}} \\ \frac{\partial g_2}{\partial m^p_{[k+1,1]}} & \frac{\partial g_2}{\partial m^p_{[k+1,2]}} & \frac{\partial g_2}{\partial m^p_{[k+1,3]}} \\ \frac{\partial g_3}{\partial m^p_{[k+1,1]}} & \frac{\partial g_3}{\partial m^p_{[k+1,2]}} & \frac{\partial g_3}{\partial m^p_{[k+1,3]}} \end{bmatrix} \begin{bmatrix} \Delta m^p_{[k,1]} \\ \Delta m^p_{[k,2]} \\ \Delta m^p_{[k,3]} \end{bmatrix} = - \begin{bmatrix} g_1(m_k, m^p_{k+1}) \\ g_2(m_k, m^p_{k+1}) \\ g_3(m_k, m^p_{k+1}) \end{bmatrix} \tag{56}$$

for the incremental update:

$$m^{p+1}_{[k+1,i]} = m^p_{[k+1,i]} + \Delta m^p_{[k,i]} \tag{57}$$

where $i = 1, 2, 3$. Equations (56) and (57) may be stated more concisely $\mathbf{J.h} = -\mathbf{g}$. Iterations continue at each timestep until: (a) a preset maximum number of iterations

Update for Body Momentum:

$$
\begin{aligned}
g_1\left(m_k, m_{k+1}\right) &= m_{[k+1,1]} - m_{[k,1]} \\
&\quad - \left[\frac{h}{4}\right]\left[\left(m_{[k,2]} + m_{[k+1,2]} + 2\cdot l_2\right)\cdot\frac{\left(m_{[k,3]} + m_{[k+1,3]}\right]}{I_3}\right) \\
&\quad + \left[\frac{h}{4}\right]\left[\left(m_{[k,3]} + m_{[k+1,3]} + 2\cdot l_3\right)\cdot\frac{\left(m_{[k,2]} + m_{[k+1,2]}\right]}{I_2}\right) \\
&= 0 \qquad (58.1)
\end{aligned}
$$

$$
\begin{aligned}
g_2\left(m_k, m_{k+1}\right) &= m_{[k+1,2]} - m_{[k,2]} \\
&\quad - \left[\frac{h}{4}\right]\left[\left(m_{[k,3]} + m_{[k+1,3]} + 2\cdot l_3\right)\cdot\frac{\left(m_{[k,1]} + m_{[k+1,1]}\right]}{I_1}\right) \\
&\quad + \left[\frac{h}{4}\right]\left[\left(m_{[k,1]} + m_{[k+1,1]} + 2\cdot l_1\right)\cdot\frac{\left(m_{[k,3]} + m_{[k+1,3]}\right]}{I_3}\right) \\
&= 0 \qquad (58.2)
\end{aligned}
$$

$$
\begin{aligned}
g_3\left(m_k, m_{k+1}\right) &= m_{[k+1,3]} - m_{[k,3]} \\
&\quad - \left[\frac{h}{4}\right]\left[\left(m_{[k,1]} + m_{[k+1,1]} + 2\cdot l_1\right)\cdot\frac{\left(m_{[k,2]} + m_{[k+1,2]}\right]}{I_2}\right) \\
&\quad + \left[\frac{h}{4}\right]\left[\left(m_{[k,2]} + m_{[k+1,2]} + 2\cdot l_2\right)\cdot\frac{\left(m_{[k,1]} + m_{[k+1,1]}\right]}{I_1}\right) \\
&= 0 \qquad (58.3)
\end{aligned}
$$

Table [2] : Dual Spin Equations in Rearranged Component Form

is reached, or (b) all changes in body momentum components from (57) are less than a preset error value times the magnitude of momentum component at the beginning of the iterations. Moreover, divergence of the iterates is avoided by ensuring $\|g\left(m_k, m_{k+1}^{p+1}\right)\|_2$ is less than $\|g\left(m_k, m_{k+1}^{p}\right)\|_2$. When this test fails, $\mathbf{h}$ is divided by powers of 2 until the norm of the new $[p+1]^{th}$ iterate is less than $\|g\left(m_k, m_{k+1}^{p}\right)\|_2$.

5.1.2 Solution of Explicit Equations for Update in Attitude

Numerical solutions to the equations in Table [1] are found by first solving (31) implicitly for m_{k+1}. From a theoretical standpoint, m_{k+1} can be explicitly substituted into (32.2), and then (32.1) for A_{k+1}. Because it is undesirable to compute the matrix inverses, solutions to (32.1) are obtained by first solving

$$\left[\mathbb{1} - \widehat{b_k}\right][x_k] = \left[\mathbb{1} + \widehat{b_k}\right] \tag{59.1}$$

for the (3×3) matrix $[x_k]$, followed by the explicit update

$$A_{k+1} = A_k \cdot [x_k]. \tag{59.2}$$

6. Implementation

The implementation of algorithms described in Sections 4.1-4.4 has been underway at the Systems Research Center since 1988 [5,22]. Initially, these simulations were written on a Silicon Graphics IRIS 3130 workstation with integrated graphical and numerical code. While this approach is satisfactory for applications that are computationally non-intensive, Sela [22] reports that increased computational power would be needed for computationally intensive applications to achieve simulation in real time. Since the IRIS Workstation has customized hardware for the Graphics, a natural solution was to develop a graphically based user interface on the IRIS for the animation, and setting up the problem description, and run the numerical simulation as a separate server process on a fast SUN workstation. InterProcess Communication Facilities [16] are used to connect the processes via Ethernet.

Design of the user interface was based on a toolkit developed by NASA-AMES [25] specifically for the Silicon Graphics IRIS workstation family. The library consists of dials, sliders, and other mouse-sensitive actuators, and panels, which are groups of actuators that appear as separate windows on the IRIS workstation.

When the program is first activated, the user interface process located on the IRIS establishes an IPC connection with the numerical simulation server, sets up a variety of panel windows for the user interface, and waits for the user to initialize simulation parameters before sending the simulation request via IPC to the numerical simulator.

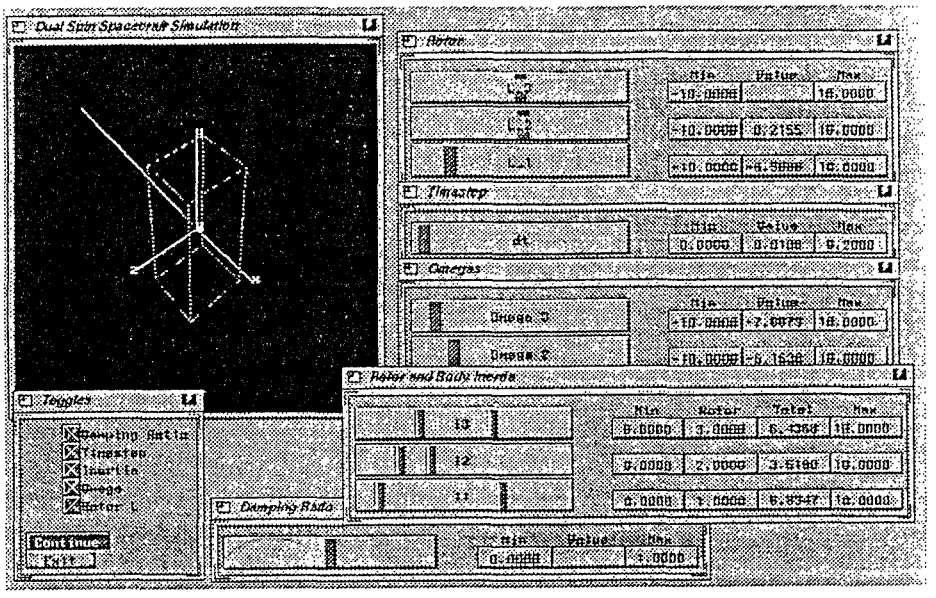

Figure [5] : User Interface for Rigid Body Simulation

Slider Name	Description
Toggles	Buttons to remove sliders from display.
Rotor	Set 3 components of angular momentum of internal rotor.
Omegas	Set 3 components of initial body angular momentum.
Timestep	Set timestep length for Midpoint Integration. Minimum and maximum startup default values are 0.0 and 0.2 seconds, respectively.
Inertia	Dual Slider to set total interia of the body, and component of rotor inertia along each axis. In all cases the rotor inertia must be less than the inertia of satellite with fixed rotors.
Damping	Set damping ratio for rotors. Notice that although equation (52) theoretically permits different damping ratios along each axis, here we assume all components of damping are identical.
Output	Displays output for time variation of Casimir, Total Energy, and each component of body angular momentum.

Table [3] : Description of User Interface Sliders

Figure [5] shows a typical screen layout for the user-interface. Individual panels containing single and groups of sliders are provided for: (a) setting the integration timestep, (b) level of damping in the rotors, (c) components of the principal moments of inertia of the combined platform and rotors, (d) principal moments of inertia of the rotors, and (e) components angular momentum for the rotors. In an effort to provide insight into the dynamical behavior of dual spin satellites, we assume for the purposes of graphical display that the satellite platform is a rectangular block whose dimensions change with adjustments to the prinicipal inertia sliders. Thus, a user becomes immediately aware that the moment of inertia sliders cannot be set in an arbitrary manner. This is because a solid rigid body must satisfy the triangle inequalities

$$I_3 \leq I_1 + I_2, \quad I_2 \leq I_3 + I_1, \quad \text{and} \quad I_1 \leq I_2 + I_3. \tag{60}$$

The interested reader is referred to Chapter 6 of Arnold [3] for details. Also displayed are the body axes for the rectangular block, and the resultant momentum vector for the internal rotors. Users quickly determine that adjustments to the matrix of damping coefficients, α, have no affect on the Casimir $C(m,d) = \|m + l + d\|^2$, but do change the rate of decay for equation (53.1). Conversly, changes to the angular momentum components for the rotors result in an almost immediate adjustment of the Casimir, with no apparent jump in the Lyapunov function decay rate.

7. Numerical Experiments

Results of numerical experiments are presented for two applications: (a) motion of a rigid body spinning freely in space, and (b) dynamics of a dual spin satellite platform containing high spinning internally damped rotors. In each case we are interested in verifying that simulations of the discrete dynamics match the theoretical predictions of Section 4.

7.1 Example 1 : Rigid Body Motion

Consider the motion of a rigid body having principal moments of inertia I = $diag\,(1,2,3)$. Initially (at time t = 0) the rigid body is spinning freely about its intermediate (unstable) axis with angular velocity $w = [1,10,1]$. 400 timesteps at $\triangle t = 0.05$ seconds are computed. At each timestep, iterations to solve the equations of motion for

body momentum m_{k+1} continue until the magnitude of the incremental updates in angular momentum components, given by equation (57), are all less than 1/100 of the component magnitudes for load vector **g** at the beginning of the iterations.

Energy and Casimir Conservation. Figure 6 shows the time variation in Energy $H(m_{k+1}) = \frac{1}{2} m_{k+1} \cdot I^{-1} m_{k+1}$ and Casimir $C(m_{k+1}) = \frac{1}{2}\|m_{k+1}\|^2$ for the rigid body. Both quantities are conserved to machine precision.

Spatial Attitute. Figures 7 and 8 show the time variation in attitude matrix component $A(1,1)$ for 400 steps of simulation at $\triangle t = 0.05$ seconds, and 4000 steps of simulation at $\triangle t = 0.005$ seconds, respectively. We recall that the role of the attitude matrix A is to describe the rotational orientation of the body frame relative to an inertial frame. As such, the time variation in all components of A is bounded by the interval $[-1, 1]$. Figures 7 and 8 match this observation. Our initial numerical experiments were with timestep $\triangle t = 0.05$. Although the Casimir and Energy were conserved to machine precision, we suspected the validity of the sharp points in the plot of $A(1,1)$ in Figure 7. To ensure that this was not an error in coding (it happens!) the simulations were repeated for the same time inteval using $\triangle t = 0.005$ seconds. The results are plotted in Figure 8. It is easy to see that time variations in peak values of attitude component $A(1,1)$ of Figure 8 are much smoother than Figure 7. However, the dramatic contraction in the period of the attitude components by merely decreasing the step length was not anticipated *apriori*. This can be seen by counting the number of cycles of $A(1,1)$ over $t \in [0, 20]$ seconds for Figures 7 and 8. The former has approximately 28.5 cycles, and Figure 8 approximately 29.3 cycles. We note that this observation is consistent with period extensions in the Newmark method; for a discussion, see Chapter 9 of Hughes [15]. Unfortunately, this observation also exposes the main weakness of the numerical approximation. While Casimirs and Energy are conserved to machine precision (indicating that the discrete dynamics follow the true trajectories in reduced phase space), we know from Section 2 that the mid-point rule is only second order accurate in computing the Poisson bracket. This translates to a systematic deviation of the discrete attitude from time-varying attitude of the continuous system. Work is currently underway to try and improve the attitude prediction by combining the mid-point rule with Richardson's Extrapolation techniques [4].

7.2 Example 2 : Dual Spin with Damping

Our second example examines the discrete time response of a dual spin statellite platform containing 3 internal rotors spinning at constant angular velocity relative to the satellite platform. Principal moments of inertia for the rotors are $I_d = diag\,(0.1, 0.1, 0.1)$. After the rotors are locked, the combined rotors plus satellite platform is assumed to have principal moments of inertia I = $diag\,(1, 2, 3)$. The internal rotor is spinning with angular momentum components $L = [0, 0, 10]$. At time t = 0, the rigid body is spinning freely about its intermediate (unstable) axis with angular velocity $w = [1, 10, 1]$. 2000 timesteps at $\triangle t = 0.05$ seconds are computed.

Conserved Quantities. Our discrete approximation to the Lyapunov function given in equation (51) asymptotically approaches a non-zero value as theoretically predicted. At the same time, the Casimir $C\,(m_{k+1}, d_{k+1}) = \|m_{k+1} + l + d_{k+1}\|^2$ is conserved to machine precision.

Spatial Attitute. Our numerical experiments conserve spatial angular momentum $\pi_{k+1} = A\,[m_{k+1} + l + d_{k+1}]$ to machine precision. As mentioned in Section 4,4, momentum transfer relies on the conservation of this quantity, and an alignment of the platform attidude along a single axis follows for high enough speeds of the driven rotors. Time variations in components of the attitide matrix $A(2, 2)$ and $A(2, 3)$ are shown in Figures 10 and 11, respectively. Although the platform is initially tumbling in an erratic manner, the effect of damping results in an alignment of the rotation about a single axis. This is inferred from component $A(2, 3)$ asymptotically approaching a single value, while component $A(2, 2)$ appears to approach a steady oscillatory motion.

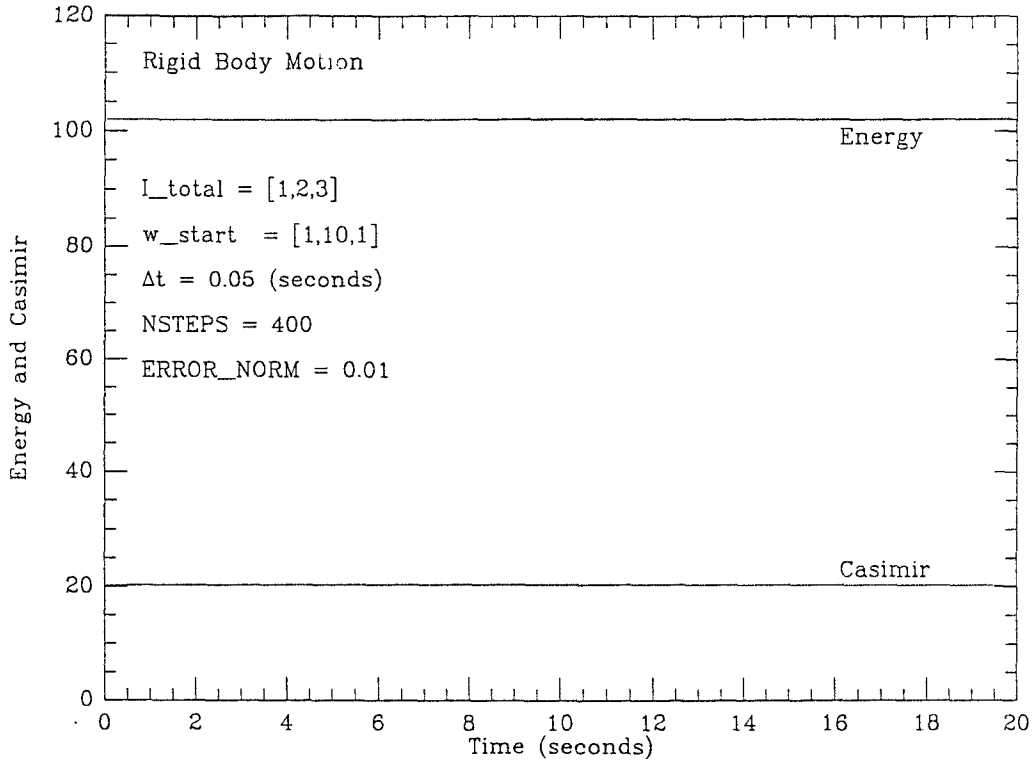

Figure [6] : Energy and Casimir for Rigid Body

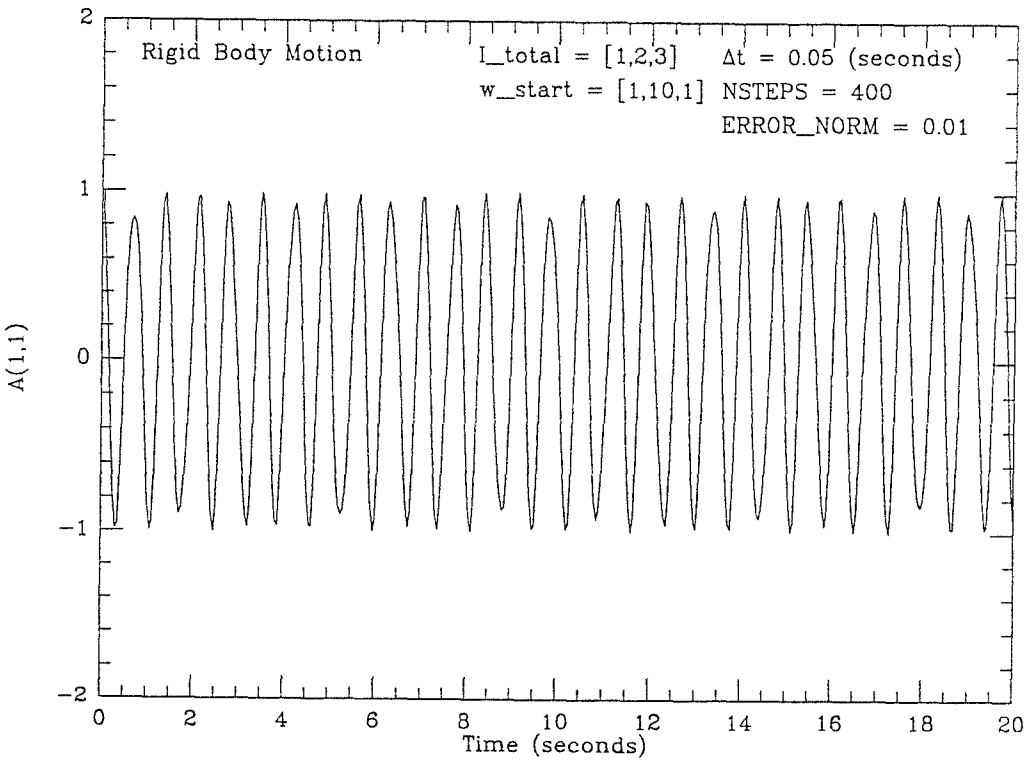

Figure [7] : A(1,1) vs Time with $\triangle t$ = 0.05 Seconds

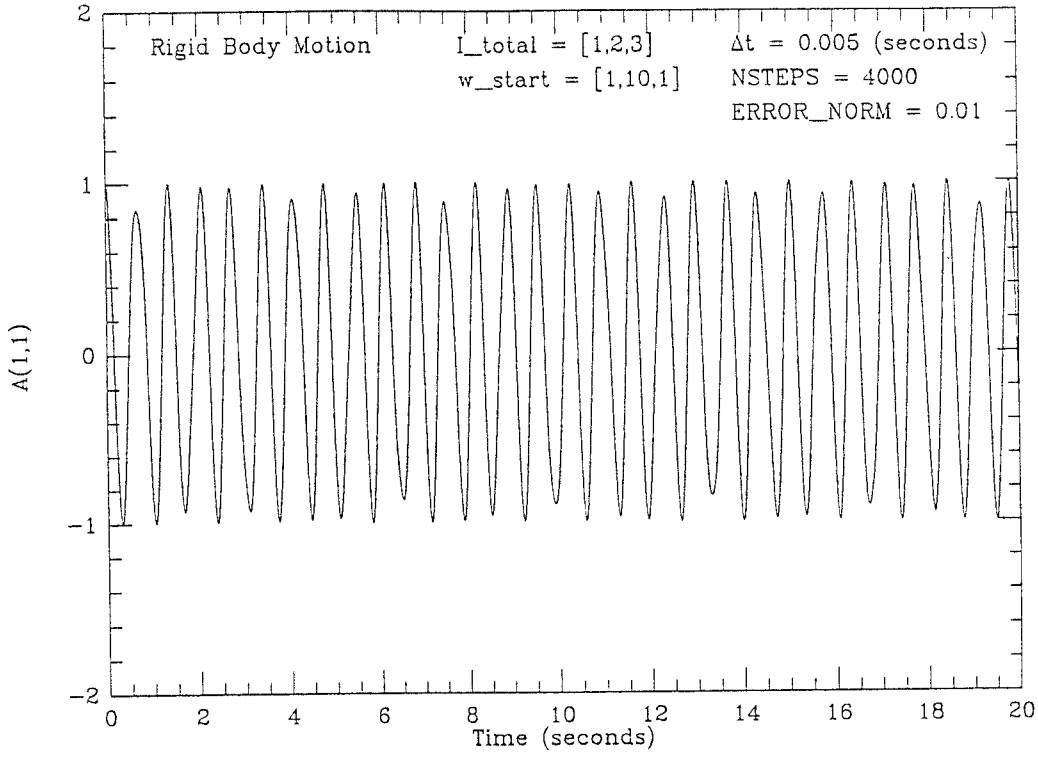

Figure [8] : A(1,1) vs Time with $\triangle t$ = 0.005 Seconds

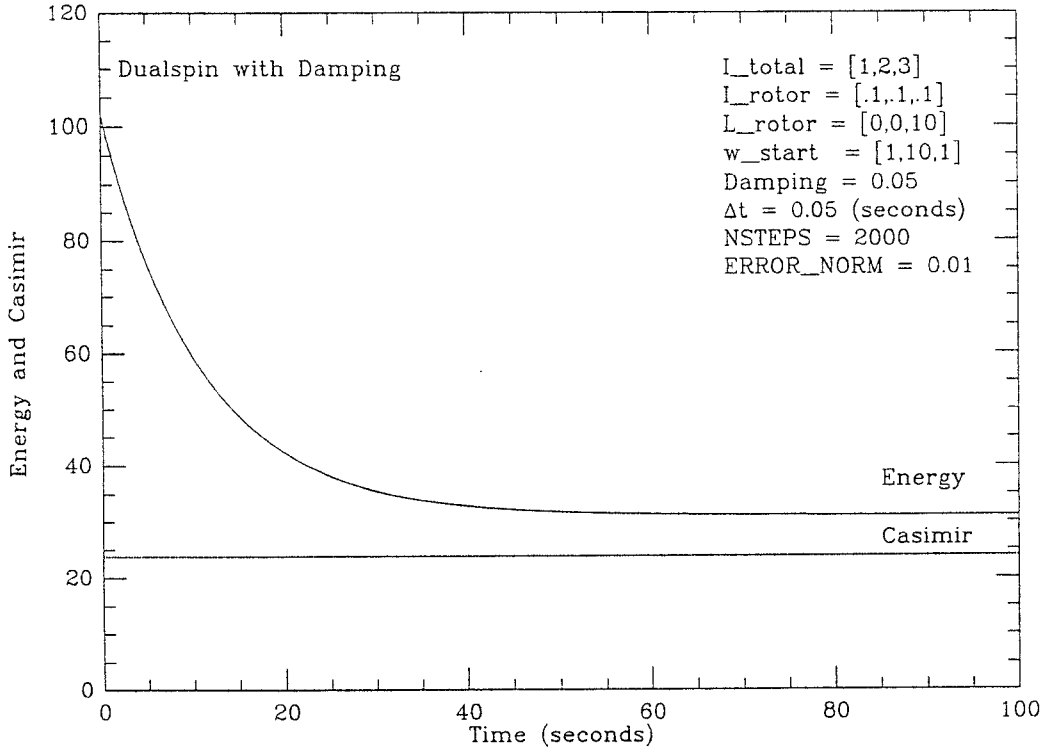

Figure [9] : Energy and Conserved Quantities vs Time for Dual Spin with Damping

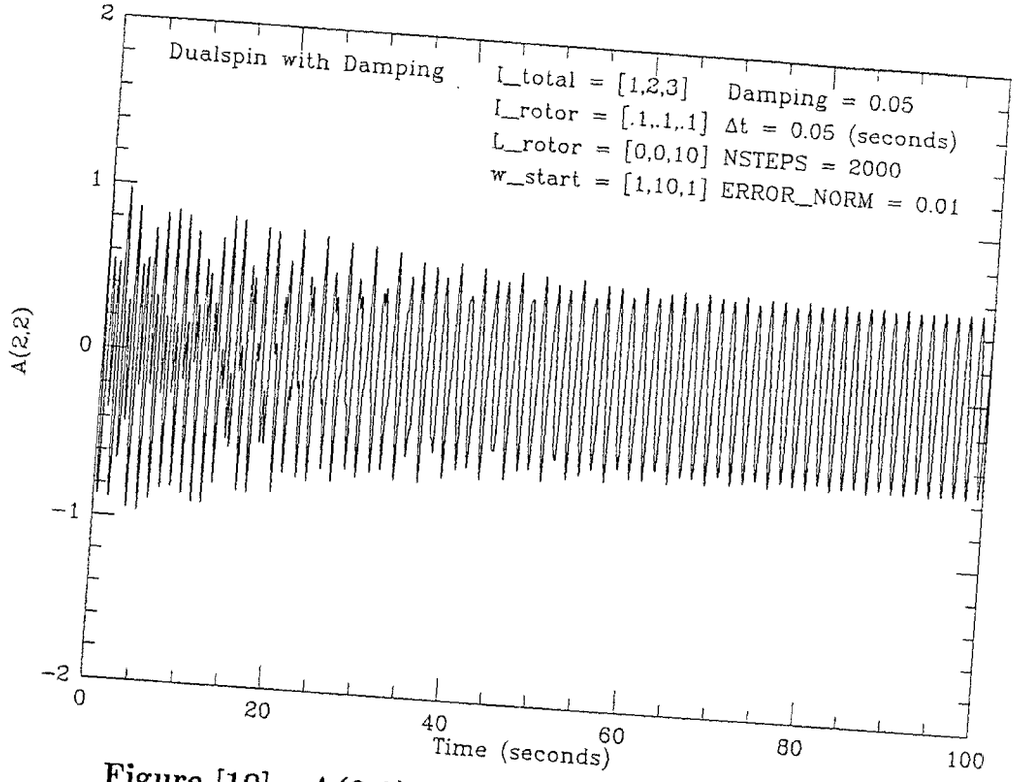

Figure [10] : A(2,2) vs Time with $\Delta t = 0.05$ Seconds

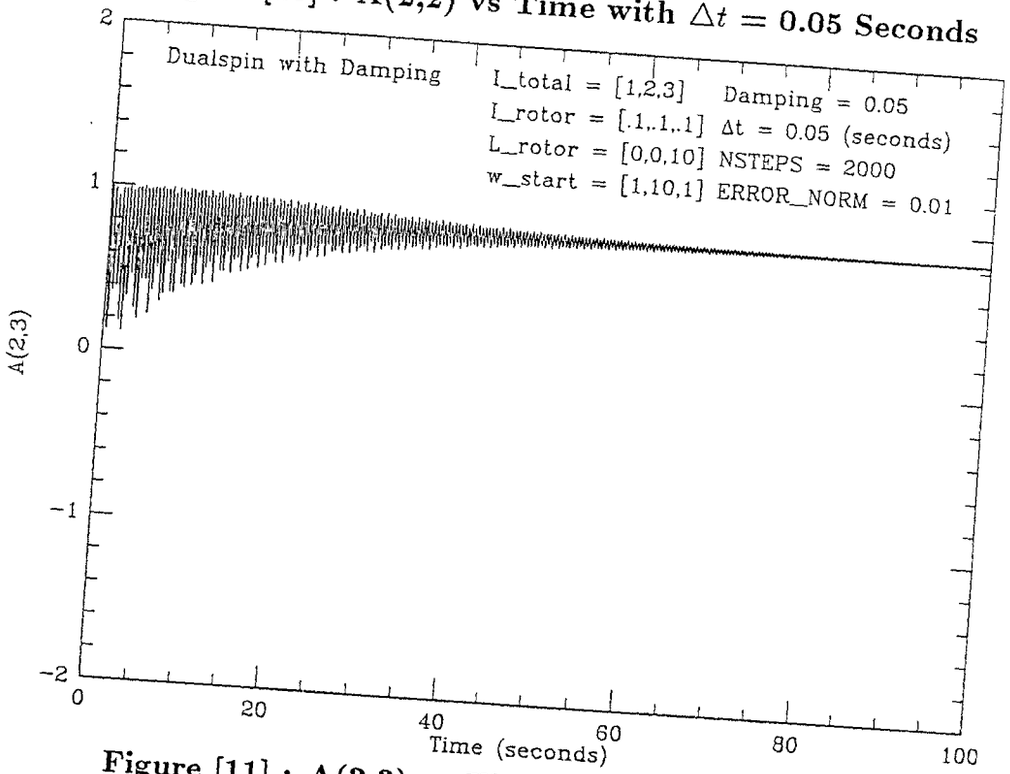

Figure [11] : A(2,3) vs Time with $\Delta t = 0.05$ Seconds

8 Conclusions

Exact solutions to the flow of a Lie-Poisson system correspond to a continuous succession of Poisson automorphisms [13], and conserve all Casimirs and the Hamiltonian (when applicable). This work has been motivated by a need to find discrete approximations to the flow that have the same properties. In particular, we have focussed on the numerical integration of Lie-Poisson systems using the mid-point rule. We have proved that the mid-point rule preserves the Poisson structure up to second order accuracy. An explicit error formula has been derived, and may be used in measuring the deviations of the Poisson structure through the approximated flow. Moreover, we have shown that any naturally conserved quantity can be approximated up to second order by using the mid-point rule. For conserved quantities containing only linear and quadratic terms such as those in the examples of this paper, the associated conservation laws are exactly satisfied.

Four rigid body systems have been studied. In each case, the dynamics in full phase space are obtained via an explicit reconstruction rule. The result is conservation of spatial angular momentum for the rigid body and dual spin satellites, and conservation of momentum along the vertical axis for the heavy top example. Indeed, the attitude acquisition of satellites containing damping rotors depends on an internal transfer of momentum, while also conserving spatial angular momentum. The behavior of dual spin satelites and rigid body applications has been animated on an IRIS workstation.

Future applications of study will include the approximations of the motion of a satellite in a central gravitational field and optimal control. Work is currently underway to try and improve the attitude prediction by combining the mid-point rule with Richardson's Extrapolation techniques [4]. In the long term, we share the view of Simo and Wong [24] that approximation precedures for the dynamics on $SO(3)$ is directly applicable to transient dynamic calculations of geometrically exact rods and shells.

References

[1] Abraham R., and Marsden J.E., **Foundations of Mechanics**, Second Edition, revised, enlarged, reset, Benjamin/Cummings, Reading.

[2] Alexander R., "Diagonally Implicit Runga-Kutta Methods for Stiff ODE's," *SIAM Journal of Num. Methods.*, Vol. 14., No. 6., December 1977.

[3] Arnold V.I. , **Mathematical Methods of Classical Mechanics**, Springer Graduate Texts in Mathematics, No. 60, Springer-Verlag, New York, 1978.

[4] Austin M.A, "High Order Integration of Smooth Dynamical Systems : Theory, Distributed Software Implementation, and Numerical Experiments," *SRC Technical Report*, Systems Research Center, University of Maryland, College Park, MD 20742, 1991 (In Preparation).

[5] Byrne R.H., "Interactive Graphics and Dynamical Simulation in a Distributed Processing Environment," *Masters Thesis*, Systems Research Center, University of Maryland, College Park, MD 20742.

[6] Channel P.J., and Scovel C., "Symplectic Integration of Hamiltonian Systems," sub. to *Nonlinearity*, June, 1988.

[7] Channel P.J., "Explicit Integration of Kick Hamiltonian in Three Degrees of Freedom," Los Alamos National Laboratory Internal Report AT-6 : ATN-86-6, 1986.

[8] Elliot D., "Time-Discretizations of Nonlinear Systems, Proceedings of the First International Conference on Systems, Washington, 1987, Ed. 6, N. DeClaris, Optimization Software Inc., N.Y., 1987.

[9] Elliot D., "Discrete-Time Systems on Manifolds," Proc. 29th IEEE CDC, Honolulu, Dec. '90 IEEE New York, pp. 1908-1909.

[10] Feng K, "Symplectic Geometry and Numerical Methods in Fluid Dynamics," Springer Lecture Notes in Physics, *Proceedings 10th Intl. Conf. Numerical Methods in Fluid Mechanics*, Beijing, 1986.

[11] Feng K, "The Symplectic Methods for Computation of Hamiltonian Systems," Springer Lecture Notes in Numerical Methods for P.D.E's, 1987.

[12] Goldstein, **Classical Mechanics**, 2nd Edition, Mc-Graw Hill, 1980.

[13] Ge-Zhong, and Marsden J., "Lie-Poisson Hamilton-Jacobi Theory and Lie-Poisson Integrators," *Phys. Lett. A.*, Vol. 133, pp. 134-139, 1989.

[14] Holmes P.J., Marsden J.E., "Horseshoes and Arnold Diffusion for Hamiltonian Systems on Lie Groups," *Indiana University Mathematics Journal*, Vol. 32, No. 2, (1983).

[15] Hughes T.J.R., **The Finite Element Method : Linear Static and Dynamic Finite Element Analysis**, Prentice-Hall Inc, 1987. pp. 803.

[16] Joy. W., Fabry R., Leffler S., **A 4.3BSD Interprocess Communication Primer**, Computer Systems Research Group, University of California, Berkeley, CA 94720.

[17] Krishnaprasad P.S., "Lie-Poisson Structure, Dual-spin Spacecraft and Asymptotic Stability," *Nonlinear Analysis, Theory, Methods and Applications*, Vol. 9, No. 10, pp. 1011-1035, 1985.

[18] Marsden J.E., Ratiu T. and Weinstein A., "Reduction and Hamiltonian Structures on Duals of Semidirect Product Lie Algebras," in J.E. Marsden et. *Fluids and Plasmas : Geometry and Dynamics* in series *Contemporary Mathematics*, Vol. 28, pp. 55-100, AMS, Providence, 1984.

[19] Marsden J.E., O'Reilly O.R., Wicklin F.J., and Zombro B.W., "Symmetry, Stability, Geometric Phases, and Mechanical Integrators," *Pre-print*, July 8, 1990.

[20] Mielke A., Holmes P., "Spatially Complex Equilibria of Buckled Rods," *Archives of Rational Mechanics and Analysis*, 1988.

[21] Sanz-Serna J.M., "Runga-Kutta Schemes for Hamiltonian Systems," BIT 28, pp. 877-883., 1988.

[22] Sela A., "Client/Server Model for Distributed Computing: An Implementation," Technical Report SRC-TR 89-7, Systems Research Center, University of Maryland, MD 20742.

[23] Simo J.C., Marsden J.E., and Krishnaprasad P.S., "The Hamiltonian Structure of Nonlinear Elasticity : The Material and Convective Representation of Rods, Plates and Shells," *Arch Rat. Mech. and Anal.*, Vol. 104, No. 2, pp. 125-183.

[24] Simo J., and Wong K.K., "Unconditionally Stable Algorithms for Rigid Body Dynamics that Exactly Preserve Energy and Momentum," *International Journal for Numerical Methods in Engineering*, Vol. 31, 1991, pp. 19-52.

[25] Tristram D.A., Walatka P.P, **Panel Library Programmers Manual**, Numerical Aerodynamic Simulation Systems Division, NASA-Ames Research Center, Moffit Field, California, 94035, April 1989.

[26] Wang Dao-Liu, "Symplectic Difference Schemes for Hamiltonian Systems on Poisson Manifolds," Computing Center, Academia Sinica, Beijing, China.

[27] Weinstein A., "The Local Structure of Poisson Manifolds," *J. Diff. Geom.*, Vol. 18, pp. 523-557 and Vol. 22, pp. 225, 1985.